Available online at www.sciencedirect.com

SciVerse ScienceDirect

Ceramics International 39 (2013) 7911–7919

CERAMICS INTERNATIONAL

www.elsevier.com/locate/ceramint

Drying of clay slabs: Experimental determination and prediction by two-dimensional diffusion models

Wilton Pereira da Silva*, Cleide Maria Diniz Pereira da Silva e Silva, Laerson Duarte da Silva, Vera Solange de Oliveira Farias

Federal University of Campina Grande, Paraiba, Brazil

Received 1 January 2013; received in revised form 14 March 2013; accepted 16 March 2013
Available online 23 March 2013

Abstract

Experiments on convective drying of clay slabs with an initial moisture content of 0.11 (dry basis, db) were performed at 50 and 90 °C. A two-dimensional numerical solution of the diffusion equation with a boundary condition of the third kind was proposed to describe the process using a constant (model 1) and variable (model 2) effective mass diffusivity value. The solution was coupled with an optimizer to determine the process parameters at each temperature using experimental datasets. The analyses of the results indicated good agreement for model 2 between each experimental dataset and the corresponding simulation.

Keywords: Effective mass diffusivity; Two-dimensional domain; Numerical simulation; Optimization

1. Introduction

The brick and roof tile industry is important in virtually every country in the world. Clay is the basic component in fabricating bricks and tiles. To manufacture these products, clay is dried, de-agglomerated and sieved. Afterward, the powder is homogenized in water, and the obtained mass is kept standing for a given amount of time. A wet product is obtained by extrusion, which is later molded into the desired shape and size. After this stage and before the sintering process, the excess water in the product is removed. As noted by Su [1], without a drying stage, the heat emanating from the sintering process will turn the water into steam inside the clay slab, which will severely damage the product. Thus, most of the water found in the product should be removed through a drying process that must be performed prior to burning.

According to Musielak and Mierzwa [2], the drying process usually influences the quality of the resulting product. It is well known that high temperatures and long drying times can significantly decrease the quality of the dried materials (change of color, permanent change in shape, inner structure damage, surface hardening, chemical changes, etc.). During drying, temperature and moisture gradients can produce stresses that generate deformations and/or cracks [1,3–6]. Consequently, a detailed description of this process is important in providing the necessary information required to produce a final item of good quality at minimal waste [7]. To describe the drying process, a mathematical model is usually used, and this model provides information that enables determining the stresses within the product [1,8,9]. Generally, water removal occurs at constant and falling rate periods [5,6,8,10]. However, depending on the value of the initial moisture content and/or the clay mineralogical content, the drying process can occur within an extremely short time period at a constant rate or only at a falling rate [7,10]. In such cases, a diffusion model can be used to describe either the entire drying process or a significant part of this process [6,7,10–12].

The definition of a diffusion model should include the following conditions: the solution is analytical [7,9,10] or numerical [6,12]; the boundary condition is of the first [9,12] or third [6,7,10] kind; and the geometry is one- [7,9,10], two- [7] or three-dimensional [6,7,12]. Recently, Silva et al. [6] described

*Corresponding author Tel.: +55 83 3333 2962.
E-mail addresses: wiltonps@uol.com.br (W.P. da Silva), cleidedps@uol.com.br (C.M.D.P. da Silva e Silva), laerson.duarte@gmail.com (L.D. da Silva), vera-solange@uol.com.br (V.S.de.Oliveira Farias).

0272-8842/$ - see front matter © 2013 Elsevier Ltd and Techna Group S.r.l. All rights reserved.
http://dx.doi.org/10.1016/j.ceramint.2013.03.053

Nomenclature

A, B, a, b	coefficients of the discretized diffusion equation or fitting parameters
C	length of slabs
D	effective mass diffusivity ($m^2\ s^{-1}$)
h	convective mass transfer coefficient ($m\ s^{-1}$)
H	height of rectangle (m)
L	thickness of rectangle (m)
M	local moisture content at time instant t (db, kg kg^{-1})
$\overline{M}$	average moisture content at time instant t (db, kg kg^{-1})
M_0	initial moisture content (db, kg kg^{-1})
M_{eq}	equilibrium moisture content (db, kg kg^{-1})
$\overline{M}_i^{exp}$	measured value of the moisture content for experimental point i (db, kg kg^{-1})
$\overline{M}_i^{sim}$	simulated moisture content for experimental point i (db, kg kg^{-1})
M_P^0	moisture content in control volume P at the beginning of a time step (db, kg kg^{-1})
N_p	number of experimental points (dimensionless)
N	number of control volumes (dimensionless)
R^2	coefficient of determination (dimensionless)
S	area (m^2)
t	drying time (s)
T	temperature (°C)
x,y	cartesian coordinates (m)
σ_i	standard deviation of experimental point i (db, kg kg^{-1})
χ^2	chi-square or objective function (dimensionless)

convective drying of clay slabs at air temperatures of 50, 60, 70, 80 and 90 °C. The initial moisture content of the product was 0.23 (db), and according to the authors, the process consisted of two periods: a constant and a falling rate. For the falling rate period, the model chosen by the authors to describe the process was a diffusive model using a three-dimensional numerical solution. The reason given by the authors for the choice of this model was that it would avoid the following simplifications: (1) the imposition of a constant value for the effective mass diffusivity (and volume) and (2) a one-dimensional representation of the clay slabs. The chosen model enabled a rigorous description of the drying process and can predict the moisture content at any position within the slab at a given instant of time. However, determining the process parameters using an optimization technique requires long time. Therefore, it seems appropriate to investigate whether a two-dimensional numerical solution of the diffusion equation can describe the process faster than the typical three-dimensional numerical solution.

The main objective of this paper is to propose a two-dimensional numerical solution for the diffusion equation in Cartesian coordinates using the finite volume method and to use the solution to describe the drying process of clay slabs.

2. Material and methods

2.1. Two-dimensional diffusion equation

The diffusion equation applied to a water migration process within a porous medium is generically written as

$$\frac{\partial M}{\partial t} = \nabla(D\,\nabla M), \tag{1}$$

where M is the moisture content ($kg_{water}\ kg^{-1}_{dry\ matter}$, dry basis, db), t is time (s) and D is the effective mass diffusivity ($m^2\ s^{-1}$). Depending on the geometry of the medium, a specific coordinate system should be chosen to solve Eq. (1). For example, for slabs, the appropriate system is Cartesian coordinates.

Many times in a diffusion process, the dimensions of the parallelepiped that represents a slab allow one to disregard the fluxes at the two smaller surfaces. In this case, to describe the process, the two-dimensional diffusion equation can be used. If there is symmetry, to save processing time and computational memory, only a quarter of the rectangle that represents the domain is studied, as shown in Fig. 1.

Observing Fig. 1, it can be seen that the mass flux in the z-direction can be disregarded when compared with the mass fluxes in the x- and y-directions. For a quarter of the rectangle, it can also be observed that due to the symmetry, the mass fluxes at the west and south boundaries are zero. In this figure, h_n and h_e represent the convective mass transfer coefficient at the north and east boundaries, respectively, and M_{eqn} and M_{eqe} represent the equilibrium moisture content at the same boundaries.

For the physical situation described above, the diffusion equation in Cartesian coordinates is given by

$$\frac{\partial M}{\partial t} = \frac{\partial}{\partial x}\left(D\frac{\partial M}{\partial x}\right) + \frac{\partial}{\partial y}\left(D\frac{\partial M}{\partial y}\right), \tag{2}$$

where x and y are the position coordinates (m).

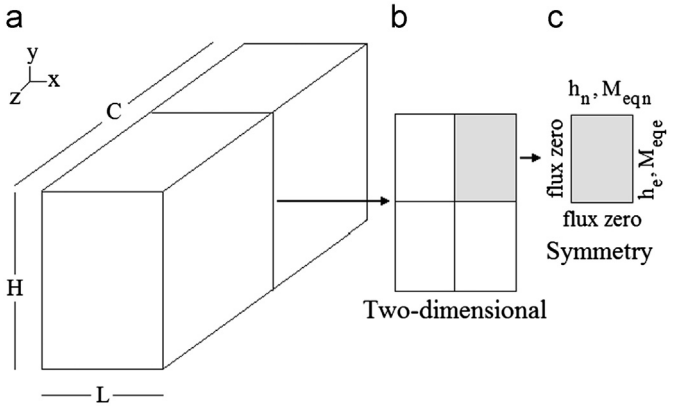

Fig. 1. (a) Parallelepiped; (b) two-dimensional slab domain and (c) symmetrical quarter of the rectangle.

The boundary condition of the third kind is expressed by imposing an equal internal diffusive flux at the boundary and an external convective flux around the vicinities of this boundary. Thus, for a two-dimensional domain, such imposition results in

$$-D\frac{\partial M(x,y,t)}{\partial c}|_b = h_b(M(x,y,t)|_b - M_{eqb}), \tag{3}$$

where c represents the x- or y-axis, and b and M_{eqb} are the position of a boundary and its equilibrium moisture content, respectively.

2.2. Numerical solution for the two-dimensional diffusion equation

If a numerical solution is used to solve the two-dimensional diffusion equation, nine types of control volumes are identified in the domain, as shown in Fig. 2(a). This figure also shows a control volume denoted "P" in a portion of the uniform grid and its neighbors to the west, east, south and north, as shown in Fig. 2(b).

The two-dimensional numerical solution will be performed in the following section using the finite volume method [13] with a fully implicit formulation.

2.2.1. Internal control volumes

For an internal control volume, after integrating Eq. (2) in space ($\Delta x\ \Delta y$) and time (from t to $t+\Delta t$), the following result is obtained for control volume P:

$$(M_P - M_P^0)\Delta x\ \Delta y = D_e\frac{M_E - M_P}{\Delta x}\Delta y\ \Delta t - D_w\frac{M_P - M_W}{\Delta x}\Delta y\ \Delta t + D_n\frac{M_N - M_P}{\Delta y}\Delta x\ \Delta t - D_s\frac{M_P - M_S}{\Delta y}\Delta x\ \Delta t, \tag{4}$$

where the subscript "0" denotes the former time t and its absence denotes the current time ($t+\Delta t$). Eq. (4) can be organized and written as follows:

$$A_P M_P = A_w M_W + A_e M_E + A_s M_S + A_n M_N + B, \tag{5}$$

in which the lowercase subscripts, "w", "e", "s" and "n", represent, the west, east, south and north boundaries, as shown in Fig. 2 the uppercase subscripts, "P", "W", "E", "S" and "N", represent nodal point P and its neighbors to the west, east, south and north (Fig. 2). The coefficients A_p, A_w, A_e, A_s, A_n and B of Eq. (5) are given by

$$A_p = \frac{\Delta x\Delta y}{\Delta t} + \frac{D_e}{\Delta x}\Delta y + \frac{D_w}{\Delta x}\Delta y + \frac{D_n}{\Delta y}\Delta x + \frac{D_s}{\Delta y}\Delta x,$$

$$A_w = \frac{D_w}{\Delta x}\Delta y; \quad A_e = \frac{D_e}{\Delta x}\Delta y; \quad A_s = \frac{D_s}{\Delta y}\Delta x;$$

$$A_n = \frac{D_n}{\Delta y}\Delta x; \quad B = \frac{\Delta x\Delta y}{\Delta t}M_P^0. \tag{6a–f}$$

In Eq. (6f), M_P^0 is the moisture content in control volume P at the beginning of time interval Δt.

2.2.2. East control volumes

For a control volume in contact with the external medium at the east boundary, integrating Eq. (2) in space and time together with the discretization of Eq. (3) adapted for the east boundary results in

$$A_P M_P = A_w M_W + A_s M_S + A_n M_N + B, \tag{7}$$

and the A_w, A_s and A_n coefficients are given by the same expressions provided in Eq. (6). Additionally, the A_p and B coefficients of Eq. (7) are given by

$$A_p = \frac{\Delta x\ \Delta y}{\Delta t} + \frac{D_w}{\Delta x}\Delta y + \frac{D_n}{\Delta y}\Delta x + \frac{D_s}{\Delta y}\Delta x + \frac{\Delta y}{(\Delta x/2D_e) + (1/h_e)},$$

$$B = \frac{\Delta x\ \Delta y}{\Delta t}M_P^0 + \frac{M_{eqe}}{(\Delta x/2D_e) + (1/h_e)}\Delta y. \tag{8a–b}$$

Integrating the diffusion equation for the other seven types of control volumes is performed with the same idea use herein. Thus, a system of equations for each time step is obtained, and this system can be solved by the Gauss–Seidel method using a tolerance of 10^{-8} for the value of M.

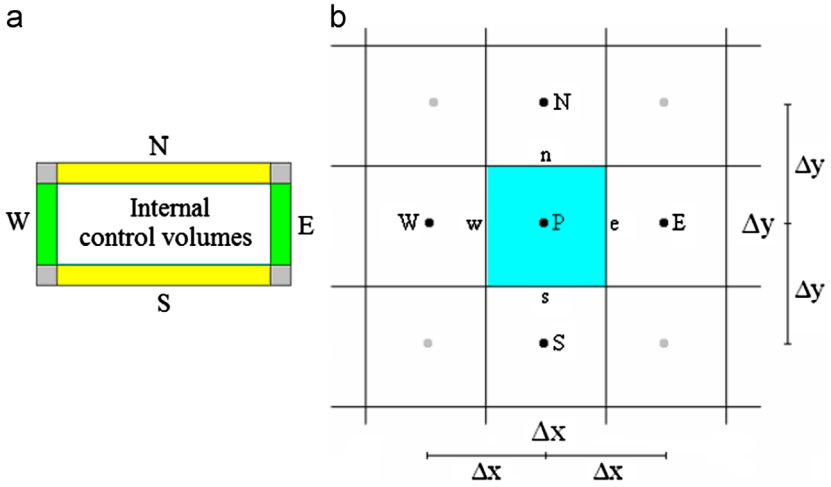

Fig. 2. (a) Types of control volumes for the two-dimensional domain; (b) control volume "P" in a portion of the uniform grid and its neighbors.

2.2.3. Average moisture content

If $M_i \equiv M(x, y, t)$ is numerically determined for all control volumes "*i*" in a given instant *t*, the average moisture content can be calculated in the following way:

$$\overline{M} = \frac{1}{S}\sum_{i=1}^{N} M_i S_i, \tag{9}$$

with

$$S = \sum_{i}^{N} S_i, \tag{10}$$

where M_i is the moisture content in control volume "*i*", S_i is the area $\Delta x\,\Delta y$ and *N* is the number of control volumes.

2.2.4. Effective mass diffusivity

The effective mass diffusivity *D* at a nodal point is calculated from a function *f* relating this parameter and the local moisture content *M*:

$$D = f(M, a, b), \tag{11}$$

where "*a*" and "*b*" are parameters that fit the numerical solution to an experimental dataset, which are determined by optimization.

For a uniform grid, on the interfaces of the control volumes, for example "*e*" (see Fig. 2), the following expression should be used to determine *D* [13]:

$$D_e = \frac{2D_E D_P}{D_E + D_P}. \tag{12}$$

According to Da Silva et al. [14], if the effective mass diffusivity is constant, the *A* coefficients in Eqs. (5) and (7) and other similar equations are calculated only once, and *B* is calculated at each time step because its value depends on M_P^0, which is the value of *M* in control volume *P* at the initial instant of each time step. However, if parameter *D* is variable, given by some function as established in Eq. (11), the *A* coefficients are also calculated at each time step due to the nonlinearities caused by the variation of the parameter. In this case, if the time refinement is adequate, errors due to the nonlinearities can be discarded.

Table 1
Drying air temperature (*T*), initial moisture content (M_0), equilibrium moisture content (M_{eq}), final moisture content (M_f), thickness (*L*), height (*H*) and length (*C*) of the clay slabs used in the optimizations.

T (°C)	M_0 (db)	M_{eq} (db)	M_f (db)	*L* (m)	*H* (m)	*C* (m)
50	0.1116	0.0162	0.0192	$6.05 \times 10{-}3$	$29.38 \times 10{-}3$	$77.50 \times 10{-}3$
90	0.1046	0.0024	0.0051	$5.92 \times 10{-}3$	$26.94 \times 10{-}3$	$77.86 \times 10{-}3$

2.2.5. General considerations and models

For the quarter rectangle, due to the symmetry, to consider the mass flux zero at the west and south boundaries, it is only necessary to impose $h_w = h_s = 0$. For the north and east boundaries, as the surfaces have the same nature and they are submitted to the same experimental conditions, a common value *h* for the convective mass transfer coefficient can be used for proposed model: $h_n = h_e = h$. In this way, the parameters "*a*" and "*b*" (effective mass diffusivity) and "*h*" (convective mass transfer coefficient) can be determined, for example, by optimization, which will be described in the following section.

To describe the drying process of clay slabs, two models using the boundary condition of the third kind were used: model 1 used a constant effective mass diffusivity, and model 2 used an effective mass diffusivity described using a function of the local moisture content.

2.3. Optimization

To determine parameters *D* and *h* by optimization for an experimental dataset, an objective function must be defined. In this article, this function is the chi-square function related to the fit of the simulated curve to the experimental dataset of the drying kinetics. The expression for the chi-square function is given by [15,16]

$$\chi^2 = \sum_{i=1}^{N_p} [\overline{M}_i^{\exp} - \overline{M}_i^{sim}]^2 \frac{1}{\sigma_i^2}, \tag{13}$$

where $\overline{M}_i^{exp}$ is the average moisture content measured at experimental point "*i*" (db), $\overline{M}_i^{\mathrm{sim}}$ is the corresponding simulated moisture content (db), N_p is the number of experimental points, and $1/\sigma_i^2$ is the statistical weight referring to point "*i*". If the statistical weights are unknown, they can be made equal to a common value, for

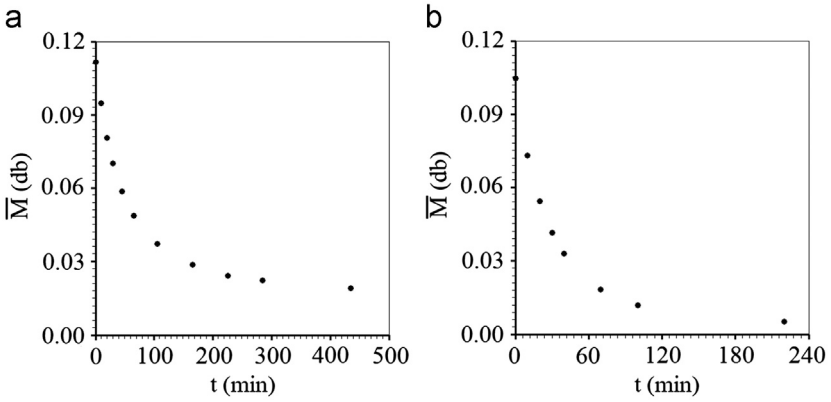

Fig. 3. Experimental datasets for drying temperature at: (a) 50 °C and (b) 90 °C.

example, 1. In Eq. (13), the chi-square value depends on $\overline{M}_i^{sim}$, which depends on D and h. If the convective mass transfer coefficient can be considered constant during the drying process and the effective mass diffusivity is given by Eq. (11), the involved parameters can be determined through the minimization of the objective function, which is accomplished in cycles involving the following steps [6,14,17]:

Step 1) Set the initial values for parameters "a", "b" and "h". Solve the diffusion equation, and determine the chi-square value.
Step 2) Set the value for the correction of "h".
Step 3) Correct parameter "h", and maintain parameters "a" and "b" at constant values. Solve the diffusion equation, and calculate the chi-square value.
Step 4) Compare the current calculated chi-square value with the previous value. If the current value is smaller, return to step 2; otherwise, decrease the last correction of the value of "h", and proceed to step 5.
Step 5) Set the value for the correction of "a".
Step 6) Correct parameter "a", and maintain parameters "b" and "h" at constant values. Solve the diffusion equation, and calculate the chi-square value.
Step 7) Compare the current calculated value of the chi-square value with the previous value. If the current value is smaller, return to step 5; otherwise, decrease the last correction value of "a", and proceed to step 8.
Step 8) Set the value for the correction of "b".
Step 9) Correct parameter "b", and maintain parameters "a" and "h" at constant values. Solve the diffusion equation, and calculate the chi-square value.
Step 10) Compare the current calculated chi-square value with the previous value. If the latest value is smaller, return to step 8; otherwise, decrease the last correction value of "b", and proceed to step 11;
Step 11) Begin a new cycle by returning to step 2 until the stipulated convergence for parameters "a", "b" and "h" is reached.

Table 2
Process parameters obtained by optimization when assuming a constant effective mass diffusivity (model 1) and the statistical indicators.

50 °C	D ($m^2\ s^{-1}$)	8.397×10^{-10}
	h ($m\ s^{-1}$)	2.708×10^{-6}
	χ^2	7.348×10^{-5}
	R^2	0.99439
90 °C	D ($m^2\ s^{-1}$)	17.256×10^{-10}
	h ($m\ s^{-1}$)	4.285×10^{-6}
	χ^2	1.766×10^{-5}
	R^2	0.99832

According to Silva et al. [6], in each cycle, the value of the correction of each parameter can be initially modest, compatible with the tolerance of the convergence imposed to the problem. For a given cycle, in each return to step 2, 5 or 8, the value of the new correction can be multiplied by a factor of 2. If the modest correction initially does not minimize the objective function, in the next cycle, its value can be multiplied by a factor of −1. In all the optimization processes, the relative tolerance on the parameters was 1.0×10^{-4}. Finally, if the effective mass diffusivity is assumed constant, steps 8–10 are unnecessary.

2.4. Experimental datasets

The raw material used in our research was red clay, which is used to make bricks and roof tiles. The raw material originated from Parelhas, a small town in the State of Rio Grande do Norte, Northeastern Brazil. The clay (41.80% SiO_2; 22.09% Al_2O_3; 10.43% Fe_2O_3; 3.79% MgO; 2.69% K_2O; 1.25% CaO and others) was dried at 110 °C, de-agglomerated in a ball mill, and sieved through an 80-mesh sieve (180 μm). The powder was homogenized with water up to a moisture content of 0.11 (db), and the obtained mass was kept standing for 24 h. Clay slabs were made by extrusion and were hand cut into slabs. The temperature and the relative humidity of the room in which the kiln was placed were, on average, 25 °C and 75%, respectively.

Two experiments to dry the clay slabs were performed using a kiln at temperatures of 50 and 90 °C. This temperature range was chosen to validate the model, covering several possibilities

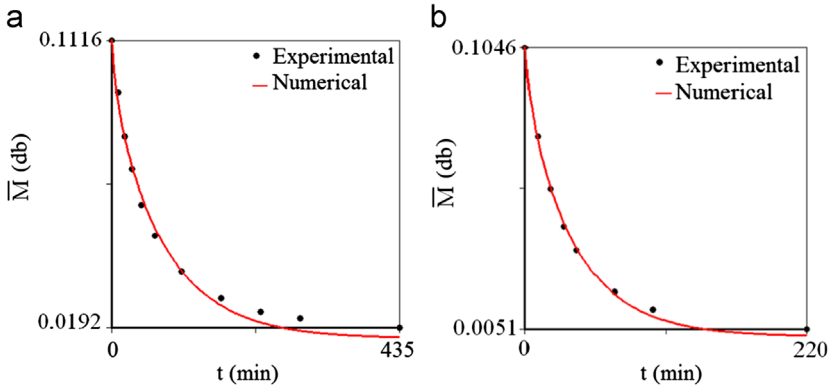

Fig. 4. Simulation of the drying kinetics predicted by model 1 with air at temperature T=: (a) 50 °C and (b) 90 °C.

of the drying process and observing the safety limits so as not to damage the product. General information about these two datasets is given in Table 1. The thickness L (m), height H (m) and length C (m) of the slabs were measured using a digital caliper. Slab measurements were taken, on average, every 20 min, and the results demonstrated that dimensional variations could be disregarded. In Table 1, M_f is the final moisture content, defining the region where the drying kinetics for each temperature was analyzed.

The moisture contents were measured by the gravimetric method, where the process continued until the mass reached its equilibrium value. At the end of each drying process, the temperature was set at 105 °C, and the slabs were kept in the kiln for 24 h, which allowed the dry matter to be measured.

The two experimental datasets related to the drying kinetics at 50 and 90 °C are presented in Fig. 3.

3. Results and discussion

3.1. Model 1: constant effective mass diffusivity

To describe the drying process using model 1 (two-dimensional with constant effective mass diffusivity), a grid with 32×32 control volumes was used, and the drying time was divided into 1000 steps. An unreported study on the grid and time refinement demonstrated that such values were appropriate to describe the process.

Table 3
Process parameters obtained by optimization when assuming a variable effective mass diffusivity (model 2) and the statistical indicators.

50 °C	D ($m^2\ s^{-1}$)	$4.463 \times 10^{-8}\ M - 5.962 \times 10^{-10}$
	h ($m\ s^{-1}$)	1.079×10^{-6}
	χ^2	1.707×10^{-6}
	R^2	0.99984
90 °C	D ($m^2\ s^{-1}$)	$7.332 \times 10^{-8}\ M + 4.042 \times 10^{-10}$
	h ($m\ s^{-1}$)	1.918×10^{-6}
	χ^2	5.173×10^{-7}
	R^2	0.99994

Optimizations were performed using model 1 for the two sets of experimental data at 50 and 90 °C. The obtained results, including the statistical indicators, are presented in Table 2.

Because the process parameters D and h have been determined, drying simulations could be performed at 50 and 90 °C, and these are presented in Fig. 4 with their respective experimental points.

3.2. Model 2: variable effective mass diffusivity

For model 2 (two-dimensional with variable effective mass diffusivity), a grid with 32×32 control volumes was also used, and the drying time was divided into 2000 steps. The A coefficients of Eqs. (5) and (7) and other similar equations were re-calculated at the end of each time step to minimize errors due to nonlinearities caused by the effective mass diffusivity variation, which influences such parameters. This error minimization was also responsible for doubling the number of time steps, from 1000 to 2000. This procedure has been considered as an alternative to using the Newton–Raphson algorithm [18].

Fig. 4 shows that after the initial time instants of the drying process, the effective mass diffusivity should be smaller than the constant value obtained with model 1. In other words, when the average moisture content decreases, the effective mass diffusivity decreases as well. Thus, in the present study, the effective mass diffusivity D is given as a function of the local moisture content M through Eq. (14), as proposed by Silva et al. [6]:

$$D = a + bM, \tag{14}$$

where a and b are parameters to be determined via optimization using the obtained experimental datasets.

For model 2, the results of the optimizations at 50 and 90 °C are summarized in Table 3, which also presents the statistical indicators related to this model.

Drying simulations were performed with the results obtained for D and h using model 2, and the drying kinetics are presented together with their respective experimental points in Fig. 5.

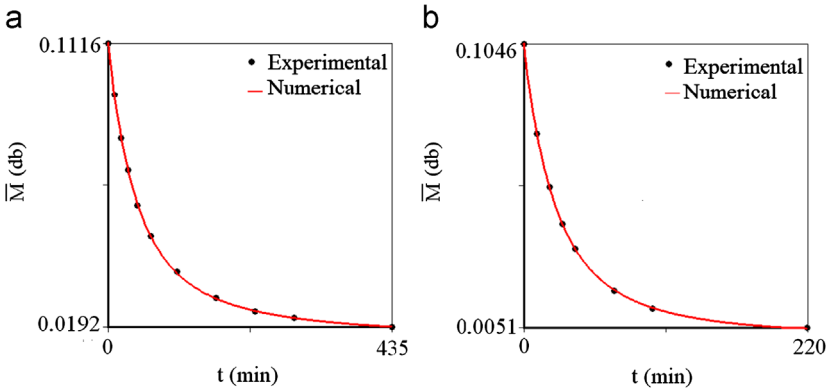

Fig. 5. Simulation of the drying kinetics predicted by model 2 with air at temperature T=: (a) 50 °C and (b) 90 °C.

A study on moisture distribution within the slab at a given instant t is important because this distribution, together with the temperature distribution, is responsible for strain and crack formation during the drying process. Model 2 provides the moisture distribution, and as an example, Fig. 6 presents this distribution at 10 and 25 min.

3.3. Comparison between models

Defining the error of experimental point "i" as

$$\text{error}_i = \overline{M}_i^{exp} - \overline{M}_i^{sim}, \quad (15)$$

the error distributions and the average errors can be presented for the two proposed models at each drying temperature, as shown in Fig. 7.

To compare the three-dimensional model and the two-dimensional model, both using a diffusivity expressed by Eq. (14), the results obtained by Silva et al. [6] for 50 and 90 °C are shown in Table 4.

Finally, the effective mass diffusivity for both the two- and three-dimensional models as a function of the local moisture content is described in Fig. 8.

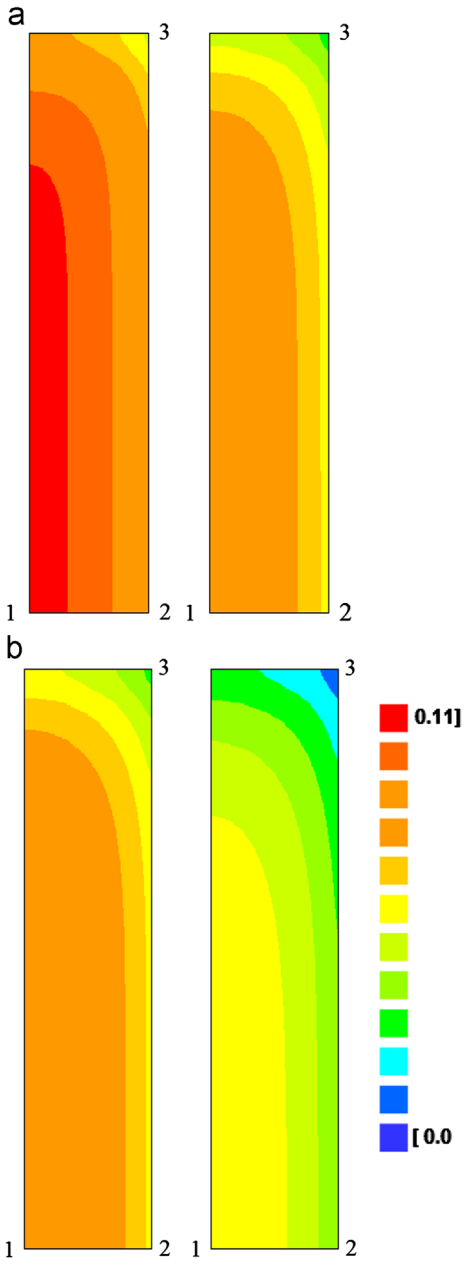

Fig. 6. Moisture distributions predicted by model 2 after 10 (left) and 25 (right) min at a drying temperature of: (a) 50 °C and (b) 90 °C.

3.4. Discussion

Considering the experimental results obtained by the present work, in which dimensional variations were disregarded, it is important to observe that similar results were obtained by Collard et al. [8] and Silva et al. [6] during the clay drying process within a range of approximately 0.11 (db) up to the final moisture content. In addition, Collard et al. [8] and Silva et al. [6], among several researchers, reported that for an initial moisture content of approximately 0.11 (db), the drying process can be described by diffusion models.

Diffusion models with constant effective mass diffusivity (or with diffusivity given as a function of the average moisture content) are abundant in literature. Such models normally use analytical solutions to describe the drying process of clay products [7,8,10,11]. However, as observed by Silva et al. [6], to avoid most restrictions encountered when using analytical solutions, numerical solutions should be preferred, as in the present study. Numerical solutions enable us, for example, to consider the effective mass diffusivity as a variable value given as a function of the local moisture content.

Inspecting Tables 2 and 3 (or Figs. 4 and 5) allows us to state that, for a given temperature, model 2 is significantly better than model 1 in describing the drying process. For example, at 50 °C for model 2, $\chi^2 = 1.707 \times 10^{-6}$, whereas for model 1, the chi-square value was $\chi^2 = 7.348 \times 10^{-5}$, which means that the factor that relates the two chi-square values is 43. Furthermore, at 90 °C, this factor is 34. With respect to determination of the coefficient, the replacement of model 1 by model 2 in the description of the drying process at 50 °C changes R^2 from 0.99439 to 0.99984, and at 90 °C, the resulting change varied from 0.99832 to 0.99994. Moreover, inspecting Fig. 7 enables us to observe that for a constant effective mass diffusivity (model 1), the error distributions are strongly biased, whereas for the variable effective mass diffusivity (model 2), the distributions can be considered random. Furthermore, at 50 °C, the average error decreases from 8.72×10^{-4} to 3.76×10^{-5} when model 1 is replaced by model 2 to describe the drying process, which means that the average error was reduced by a factor of approximately 23. At 90 °C, this reduction factor is approximately 25. Note that for the two drying temperatures, model 2 presents average errors extremely close to zero, which is the expected value for this statistical indicator.

Fig. 6 shows that during drying, the region near vertex 3 dries faster than the region 1, which corresponds to the center

of the rectangle representing the slab, as shown in Fig. 1(b). Region 2 has a drying velocity between the values obtained for regions 1 and 3. Fig. 6 also shows an expected result: for a given time instant, for example 10 (or 25) min, the greater the drying air temperature, the faster the process.

With respect to the geometry, it is expected that the two-dimensional model overestimates the process parameter D and h because the mass fluxes in the two smaller surfaces of the parallelepiped were disregarded. This result can be observed when Table 3 (two-dimensional, present article) and Table 4 (three-dimensional, Silva et al. [6]) are compared. For the two drying temperatures, model 2, as described in the present paper, overestimates the convective mass transfer coefficient in relation to the results obtained with the three-dimensional model. An inspection of Fig. 8 leads to the same conclusion for the effective mass diffusivity. Regarding the statistical indicators for the two- and three-dimensional optimizations, Tables 3 and 4 indicate that model 2, proposed in this article, is equivalent to the three-dimensional model proposed by Silva et al. [6]. Despite this equivalence, the time to perform the optimization process using model 2 is reduced by approximately eight times when compared with the time obtained by the three-dimensional model. In order to compare models, it should be borne in mind that: (1) the same optimizer, (2) the same method to solve the system of Eq. (3) and the same initial values for the parameters to be determined in the optimization processes and (4) the same tolerances for the convergences were used for the two- and three-dimensional cases. Thus, a possible explanation for such a time reduction is that model 2, as proposed in this paper, involves only 1024 control volumes (grid with 32×32 elements), whereas the three-dimensional model involves 8000 control volumes (grid $20 \times 20 \times 20$).

4. Conclusion

In this paper, drying of clay slabs with an initial moisture content of 0.11 (db) was accurately described as a diffusion phenomenon at low and high temperatures. As it was observed, model 1 (two-dimensional with constant effective mass diffusivity) could not provide a rigorous description of the process, whereas model 2 (two-dimensional with variable effective mass diffusivity) presented excellent statistical indicators in its drying process description. For model 2, the error

Table 4
Process parameters obtained by optimizing a three-dimensional model and the statistical indicators [6].

50 °C	D ($m^2\ s^{-1}$)	$3.737 \times 10^{-8}\ M - 5.085 \times 10^{-10}$
	h ($m\ s^{-1}$)	9.295×10^{-7}
	χ^2	1.710×10^{-6}
	R^2	0.99984
90 °C	D ($m^2\ s^{-1}$)	$6.503 \times 10^{-8}\ M + 2.610 \times 10^{-10}$
	h ($m\ s^{-1}$)	1.632×10^{-6}
	χ^2	4.634×10^{-7}
	R^2	0.99994

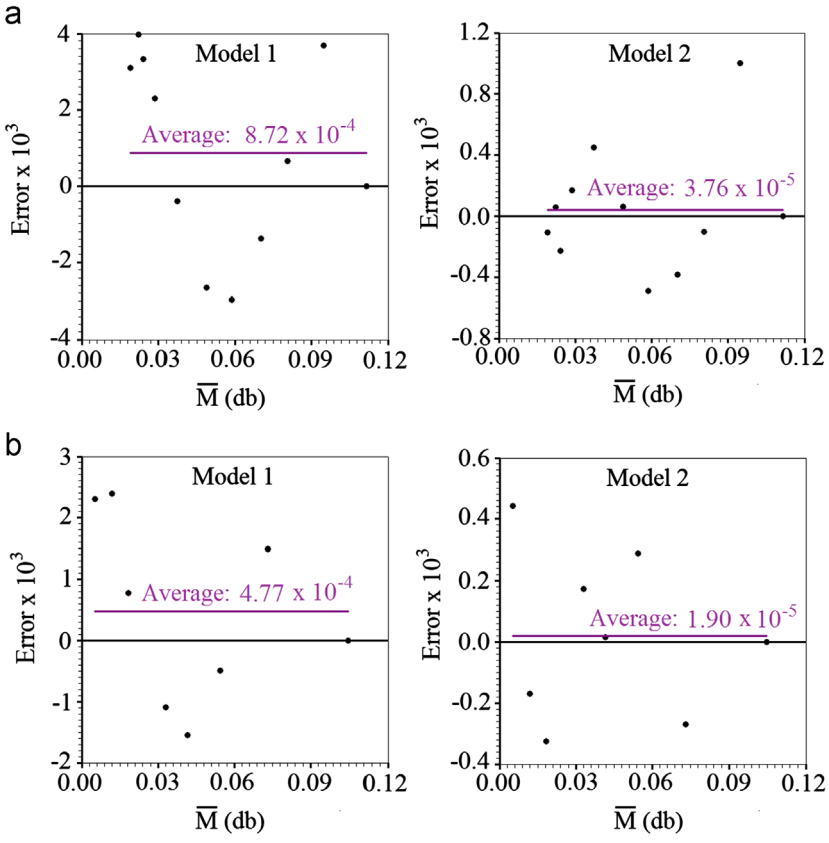

Fig. 7. Error distributions using models 1 and 2 for the simulations at temperatures: (a) 50 °C and (b) 90 °C.

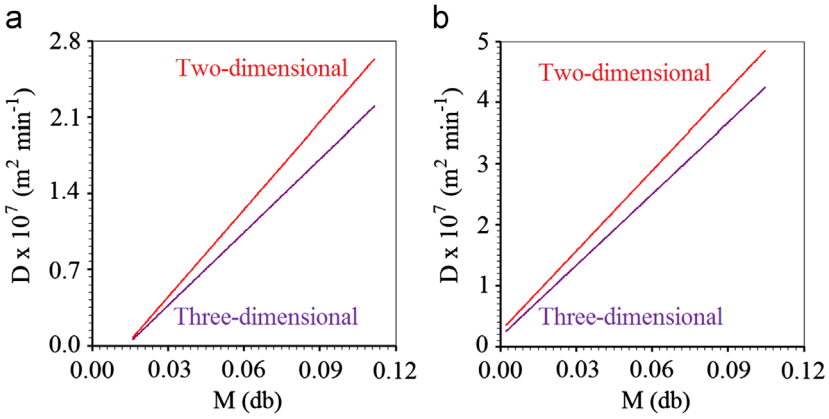

Fig. 8. Effective mass diffusivity as a function of the local moisture content for model 2 and the three-dimensional model at temperatures: (a) 50 °C and (b) 90 °C.

distributions can be considered as random. Thus, to describe the mass removal from clay slabs, one concludes that the effective water diffusivity should be expressed as a function of the local moisture content by a first-degree polynomial, where the process parameters can be determined by optimization using experimental datasets. This polynomial resulted in an increasing function that related both the effective mass diffusivity and the local moisture content. The minimum and maximum values for the effective mass diffusivity were 1.268×10^{-10} and 4.385×10^{-9} m^2 s^{-1} (at 50 °C); 5.802×10^{-10} and 8.073×10^{-9} m^2 s^{-1} (at 90 °C).

The numerical solution described in this paper for the two-dimensional diffusion equation is, in general, valid for a problem with no symmetry. In this specific case, it is only necessary to study the entire rectangle, not a symmetrical portion of it. On the other hand, a comparison between the statistical indicators of the two- and three-dimensional models makes it possible to conclude that these models are equivalent. Thus, for the case of diffusion in slabs, a two-dimensional model should be preferred due to its reduced processing time and computational memory during the optimization and simulation procedures.

Acknowledgments

We acknowledge partial financial support from the Brazilian organizations Coordenação de Aperfeiçoamento de Pessoal de Nível Superior (CAPES) and Conselho Nacional de Desenvolvimento Científico e Tecnológico (CNPq, Process number: 301697/2012-4).

References

[1] S.L. Su, Modeling of multi-phase moisture transfer and induced stress in drying clay bricks, Applied Clay Science 12 (1997) 189–207.
[2] G. Musielak, D. Mierzwa, Permanent strains in clay-like material during drying, Drying Technology 27 (2009) 894–902.
[3] G. Musielak, Possibility of clay damage during drying, Drying Technology 19 (2001) 1645–1659.
[4] R. Maciulaitis, J. Malaiškien, A. Kicait, The regulation of physical and mechanical parameters of ceramic bricks depending on the drying regime, Journal of Civil Engineering and Management 14 (2008) 263–268.
[5] D. Mihoubi, A. Bellagi, Modeling of heat and moisture transfers with stress–strain formation during convective air drying of deformable media, Heat and Mass Transfer 48 (2012) 1697–1705.
[6] W.P. Silva, L.D. da Silva, V.S.O. Farias, C.M.D.P.S. e Silva, Water migration in clay slabs during drying: a three-dimensional numerical approach, Ceramics International 39 (2013) 4017–4030.
[7] W.P. Silva, V.S.O. Farias, G.A. Neves, A.G.B. Lima, Modeling of water transport in roof tiles by removal of moisture at isothermal conditions, Heat and Mass Transfer 48 (2012) 809–821.
[8] J.M. Collard, G. Arnaud, J.P. Fohr, A. Dragon, The drying-induced deformations of a clay plate, International Journal of Heat Mass Transfer 35 (1992) 1103–1114.
[9] S. Chemkhi, F. Zagrouba, Development of a Darcy-flow model applied to simulate the drying of shrinking media, Brazilian Journal of Chemical Engineering 25 (2008) 503–514.
[10] A. Sander, D. Skansi, N. Bolf, Heat and mass transfer models in convection drying of clay slabs, Ceramics International 29 (2003) 641–653.
[11] S. Chemkhi, F. Zagrouba, Water diffusion coefficient in clay material from drying data, Desalination 185 (2005) 491–498.
[12] V.S.O. Farias, W.P. Silva, C.M.D.P.S. Silva, A.G.B. Lima, Three-dimensional diffusion in arbitrary domain using generalized coordinates for the boundary condition of the first kind: application in drying, Defect and Diffusion Forum 326–328 (2012) 120–125.
[13] S.V. Patankar, Numerical Heat Transfer and Fluid Flow, Hemisphere Publishing Corporation, New York, 1980.
[14] W.P. Da Silva, C.M.D.P.S. Silva, V.S.O. Farias, J.P. Gomes, Diffusion models to describe the drying process of peeled bananas: optimization and simulation, Drying Technology 30 (2012) 164–174.
[15] P.R. Bevington, D.K. Robinson, Data Reduction and Error Analysis for the Physical Sciences, second ed., WCB/McGraw-Hill, Boston, 1992.
[16] J.R. Taylor, An Introduction to Error Analysis, 2nd ed., University Science Books, Sausalito, California, 1997.
[17] W.P. Silva, C.M.D.P.S. Silva, P.L. Nascimento, J.E.F. Carmo, D.D.P. S. Silva, Influence of the geometry on the numerical simulation of the cooling kinetics of cucumbers, Spanish Journal of Agricultural Research 9 (2011) 242–251.
[18] W.H. Press, S.A. Teukolsky, W.T. Vetterling, B.P. Flannery, Numerical Recipes in Fortran 77. The Art of Scientific Computing, vol. 1, Cambridge University Press, New York, 1996.